Chapter 11

Free Space Optical Communication Systems

Overview: In this chapter we investigate several performance characteristics of a *free space optical* (FSO) communication system operating on a terrestrial link for which the index of refraction structure parameter C_n^2 can be treated as essentially constant. Our discussion, however, is limited to receivers operating in a *direct detection* mode.

In order to quantify the performance characteristics of a FSO communication link operating in free space, it is customary to first introduce the concept of *signal-to-noise ratio* (SNR) in the receiver system. Noise in the system includes that due to background radiation and/or noise in the receiver system itself (shot noise, circuit and electronic thermal noise, etc.). For a given SNR and threshold level, it is then possible to calculate the *probability*

of detection and *probability of false alarm.* When the link operates in the open atmosphere, we quantify the performance characteristics in terms of various *fade statistics*—the *probability of fade*, the *expected number of fades per second*, and the *mean fade time.* When the free-space SNR is sufficiently high, the most deleterious atmospheric effect on link performance is that due to *scintillation.* A reduction in scintillation on the detector, known as *aperture averaging*, can usually be achieved through the use of a large-aperture receiver. For a digital communication link operating in an atmospheric channel, it is the *probability of error* or *bit error rate* (BER) that is usually calculated from the probability of fade and probability of false alarm.

Spatial diversity in a direct detection system offers an alternative to a large-aperture receiver through the use of an array of small receiver apertures. The small apertures should be spatially separated by a sufficient distance that they detect statistically independent signals. In our analysis we compare scintillation reduction (aperture averaging) of a receiver array with that of a single large receiver lens having the same aperture area as the array of receiver lenses. The implied BER performance presented for a single-aperture receiver is likewise extended here for the receiver array system and compared with that for a single-aperture receiver system.

11.1 Introduction

In Section 1.4.1 we gave a short introduction to optical wireless communications, also called *free space optics* (FSO). All communication systems are designed to transmit and receive information, but in a FSO laser communication (*lasercom*) system the carrier frequency is selected from the much higher optical spectrum, typically on the order of 10^{14} Hz.[1] In this chapter we focus our attention primarily on FSO systems, but some of the material is applicable in regimes other than the optical regime.

Compared with conventional RF systems, there are several significant advantages offered by FSO systems that are simple consequences of the short wavelengths (high frequencies) associated with optical waves. Among these advantages are the following:

- smaller antenna (telescope)
- smaller size and weight of the components
- power concentration in a very narrow beam (a more secure channel)
- potential increase in modulation bandwidth

The last advantage is particularly important because the amount of information transmitted by a communication system is directly related to the bandwidth of

[1]The optical portion of the spectrum (see Fig. 1.8) extends roughly over wavelengths from $10^{-2}\mu$m to $10^{2}\mu$m, which includes the ultraviolet, visible, and infrared (IR) wave bands.

the modulated carrier, which is usually some fraction of the carrier frequency itself. Hence, increasing the carrier frequency to the optical spectrum has the potential to significantly increase the information capacity of a system (higher data rates). Applications that could benefit from FSO connections are those that have platforms with limited weight and space, require very high data links, and must operate in an environment where fiber-optic links are not practical such as between buildings across cities and space links.

Although FSO systems offer certain advantages over RF systems as described above, there are some drawbacks that arise from the smaller wavelengths used in FSO systems. For example:

- the high directivity of the transmitted beam makes acquisition and pointing more difficult
- optical component design requires its own technology separate from design techniques associated with RF systems (performance characteristics can be significantly different than those associated with RF systems)
- atmospheric propagation factors, such as haze, fog, rain, snow, and turbulence

Atmospheric factors are perhaps the most serious drawback to FSO because they can limit operating availability and/or cause distortions of the carrier wave that are uncommon to RF systems. Power losses associated with laser beam radiation in the visible and IR ranges can be caused by *absorption* and *scattering* of the constituent gases and particulates of the atmosphere (see Section 1.3.1). In addition, *optical turbulence* resulting from small temperature variations in the atmosphere gives rise to further power losses from spreading of the beam spot radius beyond that due to diffraction alone, and to temporal and spatial fluctuations of the laser beam known as *scintillation.* Small pointing errors can easily lead to unacceptable fade levels owing to a Gaussian roll-off in the mean irradiance profile combined with large off-axis scintillation.

A FSO communication system consists of three basic subsystems: (*i*) transmitter, (*ii*) channel, and (*iii*) receiver. The *transmitter* is composed of an encoder and modulator that prepares the information to be sent on an optical signal. The transmission medium between the transmitter and receiver collecting lens is called the *channel.* For the problems of interest to us, the channel is some portion of the atmosphere and represents the limiting factor in the performance of a FSO system. The objective of a *receiver* is to collect the transmitted optical field and process it to recover the transmitted information. A typical optical receiver consists of a front end receiving lens that focuses the light onto an optical detector where the optical field is converted into an electronic signal.

Optical receivers, briefly introduced in Section 1.5, are broadly divided into two basic types—*direct* (or *power*) *detecting receivers*, which detect only amplitude of the wave, and *coherent receivers*, which detect the wave itself (i.e., amplitude, phase, and polarization). The detector is usually followed by a postdetection processor that amplifies, processes, and eventually recovers the information from the detector output.

11.2 Direct Detection Optical Receivers

The simplest type of optical receiver for implementation is a power detecting receiver, also called a *direct* (or *noncoherent*) *detection receiver*. Because it responds only to the instantaneous power of the collected field, a direct detection receiver is used in applications when no use is made of the phase of the optical field.

In a typical model of a direct detection FSO communication system, the desired information is intensity modulated onto the optical field of a beam and transmitted through an atmospheric channel to the receiver. The receiver lens collects a portion of the transmitted optical field, which is then focused onto a photodetector surface as illustrated in Fig. 11.1. The purpose of the photodetector is to convert the focused optical field into an electrical signal for processing.

Unfortunately, the optical field is always detected in the presence of extraneous sources and noise present throughout the receiver. For example, *background radiation* (sun, blackbody radiation, etc.) is also collected by the receiving lens and focused onto the photodetecting surface along with the transmitted optical field. Background radiation at wavelengths other than that of the desired signal can be eliminated through optical filtering. These optical filters pass only certain wavelengths that determine the photodetected optical field. Background radiation at the same wavelength as the signal (or within the passband of the optical filters) is usually treated as an additive noise field to the desired optical field. Another source of noise is the photodetection process itself which produces internal interference, called *detector noise* or *shot noise*. Lastly, *circuit* and *electronic thermal noise* is generated in the processing electronics following photodetection. All electrical noise sources are treated as an additive corrupting signal.

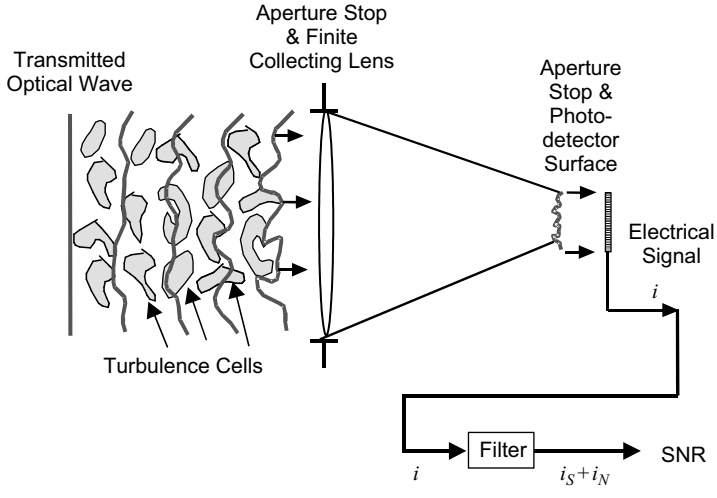

Figure 11.1 Direct detection system for a digital signal. Level "1" is the proper signal level for pulse on and Level "0" is for pulse off. Signal level above threshold when the pulse is off is a false alarm, and signal level below threshold when the pulse is on fade.

11.2.1 Threshold detection in the absence of turbulence

The need to determine the presence of a digital "signal" embedded in additive "noise" is fundamental in communication systems. There are several techniques for detecting the signal, which ordinarily rely on a *threshold* device of some kind (see Fig. 11.2). Only when the output of the detector exceeds the set threshold value do we say a *signal is present. False alarms* arise when noise alone exceeds the threshold value and is consequently interpreted as signal. On the other hand, if the signal plus noise does not exceed the threshold, it is called *missed detection* or *fade.* Threshold detection concepts are illustrated in Fig. 11.3. False alarms and threshold detection (or missed detection) involve the notion of *signal-to-noise ratio* (SNR). We discuss these concepts in this section in terms of SNR in the absence of atmospheric turbulence effects [1–4], and in Section 11.4 extend the analysis to include optical turbulence.

To begin, we note the detector in Fig. 11.1 is followed by a filter of bandwidth B, where the bandwidth is chosen to match the frequency spread of the incoming digital pulse signal-power envelope. The current flow from the filter output, induced by the incident optical wave, is

$$i = i_S + i_N, \tag{1}$$

where i_N is detector noise and i_S is the signal current defined by

$$i_S = \frac{\eta e P_S}{h\nu}. \tag{2}$$

Here, P_S is the signal power in watts, η is the detector quantum efficiency in electrons/photon (taken to be constant over the detector area), e is the electric charge in coulombs, h is Planck's constant ($h = 6.63 \times 10^{-34}$ joule-second), and ν is optical frequency in hertz. We also assume the random shot noise current i_N at the output of the filter has a zero mean so the total noise power is defined by

$$\sigma_N^2 = \langle i^2 \rangle - \langle i \rangle^2 = \langle i_N^2 \rangle, \tag{3}$$

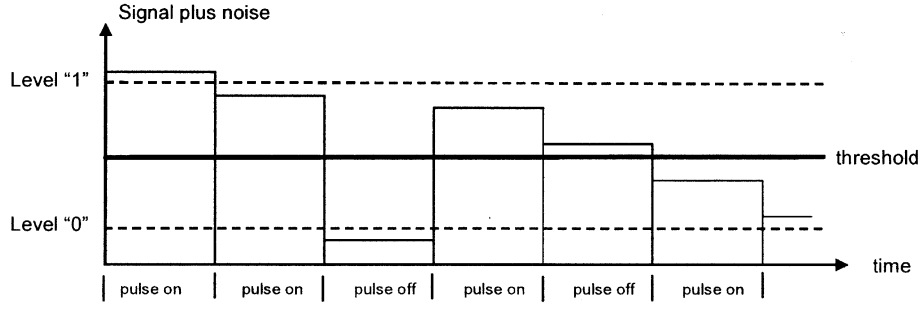

Figure 11.2 Threshold setting for a digital signal. Level "1" is the proper signal level for pulse on and Level "0" is for pulse off. Signal level above threshold when the pulse is off is a false alarm, and signal level below threshold when the pulse is on is a fade.

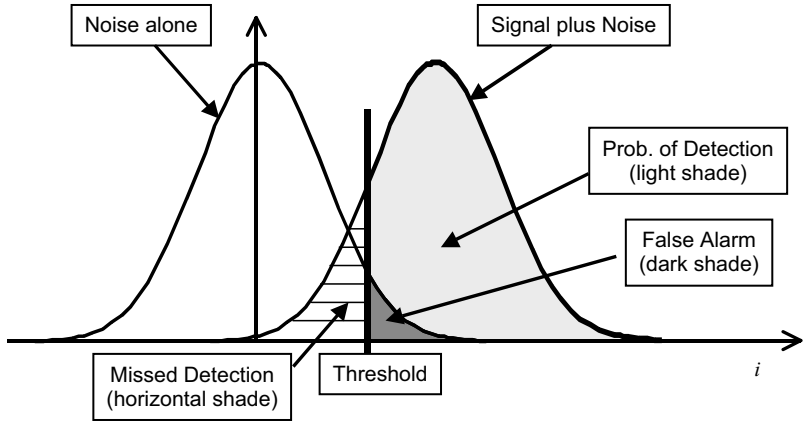

Figure 11.3 Probability of detection and false alarm.

where the mean-square noise value is (ignoring background light and other noise sources)

$$\langle i_N^2 \rangle = 2eBi_S = \frac{2\eta e^2 BP_S}{h\nu}. \tag{4}$$

Hence, the detector current noise power is proportional to signal current (or power). We define the output SNR (in the absence of optical turbulence) by the ratio of the detector signal current i_S to the root-mean-square (rms) noise current σ_N, which yields

$$\mathrm{SNR}_0 = \frac{i_S}{\sigma_N} = \sqrt{\frac{\eta P_S}{2h\nu B}}. \tag{5}$$

Because we have ignored background illumination, circuit, and thermal noise, the SNR (5) is called *shot-noise* (or *photon-noise*) *limited.*

When signal levels are low in the photon-counting regime, it is customary to use poisson statistics for describing the random noise when other noise sources are negligible. Here, however, we will assume that the mean photo count is sufficiently large that Gaussian statistics can apply for *all* noise sources. In this case, we designate the SNR by

$$\mathrm{SNR}_0 = \frac{i_S}{\sigma_N}, \tag{6}$$

and the probability density function (PDF) for random noise is described by the zero-mean Gaussian distribution

$$p_n(i) = \frac{1}{\sqrt{2\pi}\sigma_N} \exp\left(-\frac{i^2}{2\sigma_N^2}\right). \tag{7}$$

The total output current i from the filter containing both signal and noise has mean value i_S, and therefore, the total current is governed by the nonzero-mean Gaussian PDF

$$p_{s+n}(i) = \frac{1}{\sqrt{2\pi}\sigma_N} \exp\left[-\frac{(i - i_S)^2}{2\sigma_N^2}\right]. \tag{8}$$

The *probability of detection* and *probability of false alarm* are given, respectively, by

$$\mathrm{Pr_d} = \int_{i_T}^{\infty} p_{s+n}(i)\, di = \frac{1}{2}\mathrm{erfc}\left(\frac{i_T - i_S}{\sqrt{2}\sigma_N}\right), \tag{9}$$

$$\mathrm{Pr_{fa}} = \int_{i_T}^{\infty} p_n(i)\, di = \frac{1}{2}\mathrm{erfc}\left(\frac{i_T}{\sqrt{2}\sigma_N}\right), \tag{10}$$

where erfc(x) is the complementary error function (see Appendix I).

The SNR is a common measure of system performance, but a better performance measure in digital communications is provided by the *probability of error*, also called the *bit error rate* (BER), which depends on SNR. The most basic form of pulsed modulation in digital communications is on-off keying (OOK). Each bit symbol is transmitted by pulsing the source either on or off during each bit period. Because of random noise, a transmitted 0 may be mistaken for a 1, which we denote by Pr(1|0), and a 1 may be mistaken for a 0, denoted by Pr(0|1). Assuming each symbol is equally likely to be sent, the BER is given by

$$\Pr(E) = \frac{1}{2}\Pr(1|0) + \frac{1}{2}\Pr(0|1) = \frac{1}{2}\mathrm{erfc}\left(\frac{\mathrm{SNR}_0}{2\sqrt{2}}\right), \tag{11}$$

where SNR_0 is defined by (6) and we have set $i_T = 0.5 i_S$, consistent with conventional treatments of BER with noise alone. Here, Pr(1|0) is the probability of false alarms (10) and Pr(0|1) is missed detection (fade) defined by $1 - \mathrm{Pr_d}$.

11.2.2 Frequency of fades and surges

We define the *probability of miss* or *fade* below threshold by $\mathrm{Pr_{fade}} = 1 - \mathrm{Pr_d}$, where $\mathrm{Pr_d}$ is the probability of detection (9). The fade probability provides us with an estimate of how likely the output current i from the detector is to drop below a prescribed threshold i_T. Related quantities of interest are the *frequency of surges* and *frequency of fades* of the output current, which are identical with the frequency of positive and negative crossings of the threshold level, i.e., the slope of the current i.

For a stationary process, Rice [5,6] has shown that the frequency of either positive or negative crossings of the threshold value i_T by the output current is given by the *expected number of crossings per second* defined by

$$\langle n(i_T)\rangle = \frac{1}{2}\int_{-\infty}^{\infty} |i'| p_{s+n}(i_T, i')\, di', \tag{12}$$

where $p_{s+n}(i, i')$ is the joint PDF of the output current i and its time derivative i'. Rice has also shown that the time derivative of a random process and the

process itself are uncorrelated, but not necessarily independent. However, the time derivative of a Gaussian process is another Gaussian process and, hence, is therefore statistically independent of the original process.

The output current of a direct detection system has the Gaussian distribution (8), and the joint PDF of the current i and its time derivative i' is given by the product of marginal Gaussian distributions [5,6]

$$p_{s+n}(i, i') = p_i(i)p_{i'}(i') = \frac{1}{\sqrt{2\pi b_0}}\exp\left[-\frac{(i-i_S)^2}{2b_0}\right]\frac{1}{\sqrt{2\pi b_2}}\exp\left(-\frac{i'^2}{2b_2}\right), \quad (13)$$

where

$$\begin{aligned} b_0 &= \sigma_N^2 = \frac{1}{2\pi}\int_0^\infty S_N(\omega)\, d\omega, \\ b_2 &= \frac{1}{2\pi}\int_0^\infty \omega^2 S_N(\omega)\, d\omega. \end{aligned} \quad (14)$$

The quantity $S_N(\omega)$ in (14) is the power spectrum of the noise current and ω is angular frequency. Here, $b_0 = \sigma_N^2$ is recognized as the noise power and, consequently, the related quantity b_2 is the autocorrelation function of the time derivative of the random noise evaluated at $t = 0$ [7]. Based on (12) and (13), we are led to

$$\langle n(i_T)\rangle = \frac{1}{2\pi}\sqrt{\frac{b_2}{b_0}}\exp\left[-\frac{(i_T-i_S)^2}{2b_0}\right] = \nu_0\exp\left[-\frac{(i_T-i_S)^2}{2\sigma_N^2}\right], \quad (15)$$

where $\nu_0 = \sqrt{b_2/b_0}/2\pi$, called a *quasi-frequency*, is the frequency of fades when $i_T = i_S$; thus, ν_0 provides a measure of the effective bandwidth of i.

When the signal current $i_S = 0$, the expected number of surges (or fades) (15) reduces to the *false-alarm rate* (FAR)

$$\text{FAR} = \frac{B}{2\sqrt{3}}\exp\left(-\frac{i_T^2}{2\sigma_N^2}\right), \quad (16)$$

where B is the bandwidth (positive frequencies only) of the low-pass filter in Fig. 11.1.

Note that both the false alarm probability (10) and the FAR (16) depend on the *threshold-to-noise ratio* (TNR) defined by

$$\text{TNR} = \frac{i_T}{\sigma_N}. \quad (17)$$

Ordinarily, the desired FAR (16), or the probability of false alarm (10), is specified in a FSO communication system in order to achieve a particular system performance level. If the FAR is specified, the TNR is a function of FAR given by

$$\text{TNR} = \sqrt{2\ln\left(\frac{B}{2\sqrt{3}\text{FAR}}\right)}, \quad (18)$$

and if the probability of false alarm is specified, then Eq. (10) sets the TNR as a function of Pr_{fa}. In Fig. 11.4 we plot TNR (18) as a function of FAR/B. Consequently, if we specify $\text{FAR}/B = 10^{-12}$, it follows from (18) that $\text{TNR} = 7.26$.

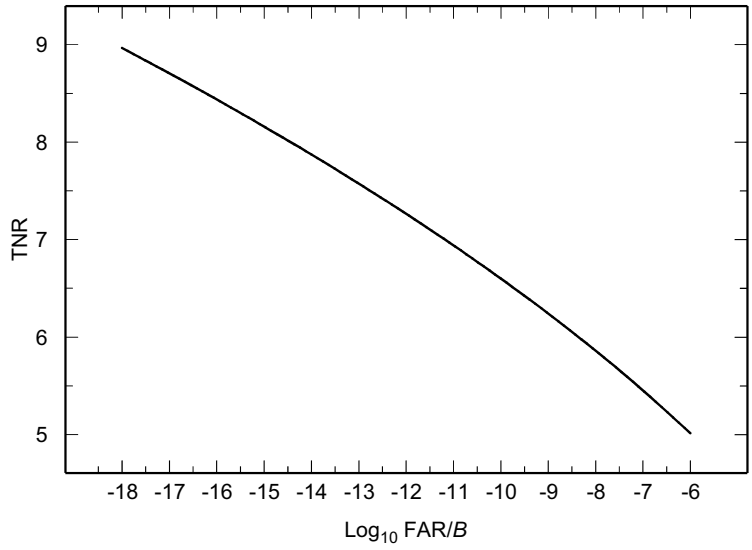

Figure 11.4 Threshold-to-noise ratio (TNR) as a function of FAR/B.

11.3 Fade Statistics—Part I

The application areas for FSO systems are numerous. In particular, FSO links are being strongly considered by various branches of the military for supporting all tactical operations. However, the performance of a FSO system can be significantly diminished by turbulence-induced scintillation resulting from beam propagation through the atmosphere. Specifically, scintillation can lead to power losses at the receiver and eventually to fading of the received signal below a prescribed threshold. The reliability of a FSO system operating in such an environment can be deduced from a mathematical model for the probability density function (PDF) of the randomly fading irradiance signal. From knowledge of this PDF model, we can calculate the *probability of fade* (or missed detection), the *expected number of fades* below a prescribed threshold, and the average time at which the signal stays below the threshold called the *mean fade time.*

In the distribution model developed in Section 9.10 we assumed that large-scale and small-scale factors in the (normalized) irradiance $I = XY$ are statistically independent, and further, that each is governed by a *gamma distribution*, viz.,

$$\begin{aligned} p_X(X) &= \frac{\alpha(\alpha X)^{\alpha-1}}{\Gamma(\alpha)}\exp(-\alpha X), \qquad X > 0, \\ p_Y(Y) &= \frac{\beta(\beta Y)^{\beta-1}}{\Gamma(\beta)}\exp(-\beta Y), \qquad Y > 0, \end{aligned} \tag{19}$$

where α and β are positive parameters directly related to the large-scale and small-scale scintillations of the optical wave according to

$$\alpha = \frac{1}{\sigma_X^2} = \frac{1}{\exp(\sigma_{\ln X}^2) - 1},$$
$$\beta = \frac{1}{\sigma_Y^2} = \frac{1}{\exp(\sigma_{\ln Y}^2) - 1}. \tag{20}$$

For the case of a point receiver (or pupil plane analysis), we showed in Section 9.10 that the PDF for the irradiance, resulting from the assumptions given above in (19), leads to the *gamma-gamma distribution* [see Eq. (138) in Chap. 9].

In the presence of a finite receiver aperture (see Fig. 11.5), it is customary to assume the PDF model for the irradiance in the plane of the photodetector at distance $L + L_f$ from the transmitter is from the same general family as that in the pupil plane at distance L from the transmitter. This is equivalent to stating that power fluctuations over a large receiver aperture and the pupil plane irradiance at a point can be modeled by the same family of PDFs. Although this may not strictly be the case, in the following analysis we will follow this custom and assume the irradiance in the plane of the photodetector is from the same family as in the pupil plane, taking into account the change in mean irradiance and power fluctuations (flux variance).

Based on the above discussion, we will assume the governing PDF in the plane of the photodetector under all irradiance fluctuation conditions is given by the gamma-gamma PDF

$$p_I(I) = \frac{2(\alpha\beta)^{(\alpha+\beta)/2}}{\Gamma(\alpha)\Gamma(\beta) I} \left(\frac{I}{\langle I(0, L + L_f) \rangle} \right)^{(\alpha+\beta)/2} K_{\alpha-\beta}\left(2\sqrt{\frac{\alpha\beta I}{\langle I(0, L + L_f) \rangle}} \right), \quad I > 0, \tag{21}$$

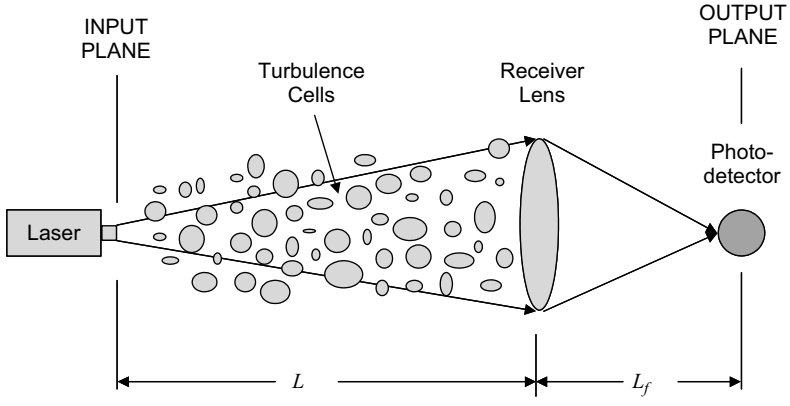

Figure 11.5 Propagation geometry for a Gaussian beam originating at distance L to the left of a thin Gaussian lens of real focal length F_G and effective transmission radius W_G.

where we are taking the general case of mean irradiance $\langle I(0, L + L_f)\rangle \neq 1$ and $K_v(x)$ is a modified Bessel function. In writing this expression we are neglecting any possible pointing error. Traditionally, the PDF most often used under *weak irradiance fluctuations* is the lognormal model

$$p_I(I) = \frac{1}{I\sigma_I(0, L + L_f)\sqrt{2\pi}} \exp\left\{ - \frac{\left[\ln\left(\frac{I}{\langle I(0, L + L_f)\rangle}\right) + \left(\frac{1}{2}\right)\sigma_I^2(0, L + L_f)\right]^2}{2\sigma_I^2(0, L + L_f)} \right\}, \quad I > 0, \tag{22}$$

where $\sigma_I^2(0, L + L_f) = \sigma_I^2(D_G)$ is the flux variance in the plane of the detector and where we are showing dependency upon the aperture diameter of the receiver D_G. Below, we illustrate some fade probability results based on the lognormal model in addition to those based on the gamma-gamma distribution, even though it is believed the lognormal model generally predicts optimistic fade probabilities [8–12]. That is, the behavior of the lognormal model in the tail for small values of I does not agree with simulation data for either an infinite plane wave or spherical wave (e.g., see Sections 9.10.1 and 9.10.2), and this is the most critical area for calculating fade probabilities.

In this section we treat the signal-to-noise ratio (SNR) at the output of the detector system sufficiently high that the fading statistics can be based wholly on statistics associated with the irradiance of the received signal. In such cases, we make no distinction between direct detection or coherent detection receiver systems.

11.3.1 Probability of fade

Given a PDF model for irradiance fluctuations $p_I(I)$, the *probability of fade* describes the percentage of time the irradiance of the received wave is below some prescribed threshold value I_T. Hence, the probability of fade as a function of threshold level is defined by the cumulative probability

$$P(I \leq I_T) = \int_0^{I_T} p_I(I)\, dI. \tag{23}$$

For the lognormal PDF (22), the resulting probability of fade leads to

$$\Pr(I \leq I_T) = \frac{1}{2}\left\{ 1 + \operatorname{erf}\left[\frac{\left(\frac{1}{2}\right)\sigma_I^2(0, L + L_f) - 0.23F_T}{\sqrt{2}\sigma_I(0, L + L_f)} \right] \right\}, \tag{24}$$

where $\operatorname{erf}(x)$ is the error function. In arriving at this expression we have introduced the *fade threshold parameter*

$$F_T = 10\log_{10}\left(\frac{\langle I(0, L + L_f)\rangle}{I_T}\right). \text{ [dB]} \tag{25}$$

The fade parameter F_T, given in decibels (dB), represents the dB level *below* the on-axis mean irradiance that the threshold I_T is set.

From the gamma-gamma distribution (21), the corresponding cumulative distribution is [12]

$$\begin{aligned}\Pr(I \le I_T) = \frac{\pi}{\sin[\pi(\alpha-\beta)]\Gamma(\alpha)\Gamma(\beta)} \Bigg\{ & \frac{(\alpha\beta)^{\beta}}{\beta\Gamma(\beta-\alpha+1)} \exp(-0.23F_T\beta) \\ & \times {}_1F_2\big[\beta;\, \beta+1, \beta-\alpha+1;\ \alpha\beta\exp(-0.23F_T)\big] \\ & - \frac{(\alpha\beta)^{\alpha}}{\alpha\Gamma(\alpha-\beta+1)} \exp(-0.23F_T\alpha) \\ & \times {}_1F_2\big[\alpha;\ \alpha+1, \alpha-\beta+1;\ \alpha\beta\exp(-0.23F_T)\big] \Bigg\},\end{aligned} \tag{26}$$

where ${}_1F_2$ denotes a generalized hypergeometric function (see Appendix I). Although (26) is an exact result, current software programs can lead to numerical errors in the calculation of the generalized hypergeometric functions for certain values of the argument (particularly for large arguments). To avoid such possibilities, it may be better in some cases to numerically integrate the PDF in Eq. (21).

In Figs. 11.6–11.8 we show the probability of fade associated with a Gaussian-beam wave as a function of fade threshold parameter F_T. Results are presented for both the lognormal model and the gamma-gamma PDF, using the Kolmogorov power-law spectrum. The fade probabilities are based on a point receiver ($D_G \cong 0$) and also on a large-aperture receiver in which the aperture diameter $D_G = 4$ cm, the latter case leading to aperture averaging effects (see Section 10.3). In our analysis we assume that beam-wander-induced scintillation is negligible.

Parameters α and β for the gamma-gamma PDF are defined in general by Eqs. (20). When aperture averaging effects are taken into account, these parameters are given by

$$\alpha = \frac{1}{\exp[\sigma^2_{\ln X}(D_G)] - 1}, \quad \beta = \frac{1}{\exp[\sigma^2_{\ln Y}(D_G)] - 1}, \tag{27}$$

and the flux variance of irradiance fluctuations is

$$\sigma_I^2(0,\, L + L_f) = \exp\big[\sigma^2_{\ln X}(D_G) + \sigma^2_{\ln Y}(D_G)\big] - 1, \tag{28}$$

where the large-scale and small-scale log-irradiance variances are (recall Section 10.3.5)

$$\sigma^2_{\ln X}(D_G) = \frac{0.49\left(\dfrac{\Omega_G - \Lambda_1}{\Omega_G + \Lambda_1}\right)^2 \sigma_B^2}{\left[1 + \dfrac{0.4(2-\overline{\Theta})(\sigma_B/\sigma_R)^{12/7}}{(\Omega_G + \Lambda_1)\left(\dfrac{1}{3} - \dfrac{1}{2}\overline{\Theta}_1 + \dfrac{1}{5}\overline{\Theta}_1^2\right)^{6/7}} + 0.56(1+\Theta_1)\sigma_B^{12/5}\right]^{7/6}}, \tag{29}$$

$$\sigma^2_{\ln Y}(D_G) = \frac{0.51\sigma_B^2(\Omega_G + \Lambda_1)\left(1 + 0.69\sigma_B^{12/5}\right)^{-5/6}}{\Omega_G + \Lambda_1 + 1.20(\sigma_R/\sigma_B)^{12/5} + 0.83\,\sigma_R^{12/5}}. \tag{30}$$

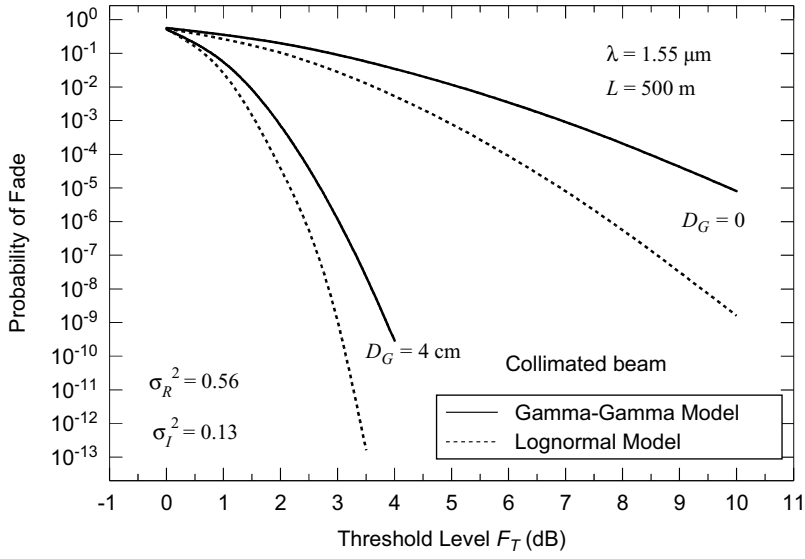

Figure 11.6 Probability of fade as a function of threshold level below the mean under weak irradiance fluctuation conditions ($\sigma_R^2 < 1$). Inner scale and outer scale, respectively, are assumed to be $l_0 = 0$ and $L_0 = \infty$, and D_G is the diameter of the receiver aperture.

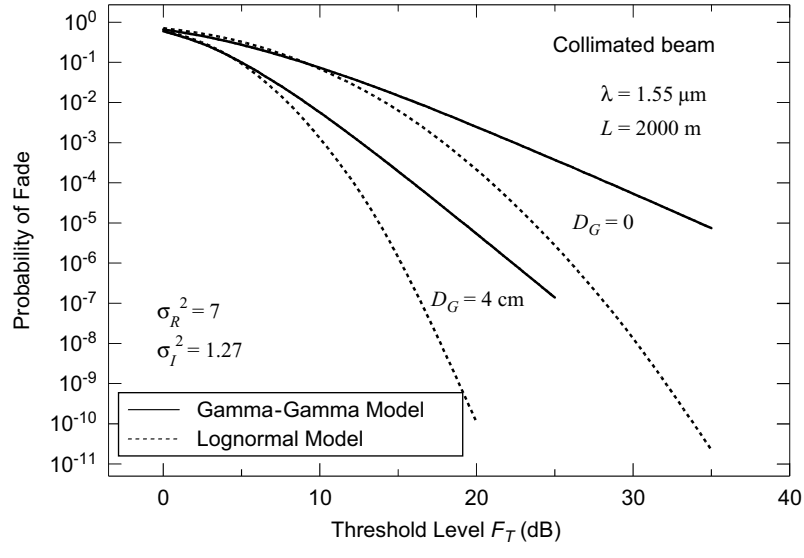

Figure 11.7 Same as Fig. 11.6 except under moderate irradiance fluctuation conditions ($\sigma_R^2 > 1$).

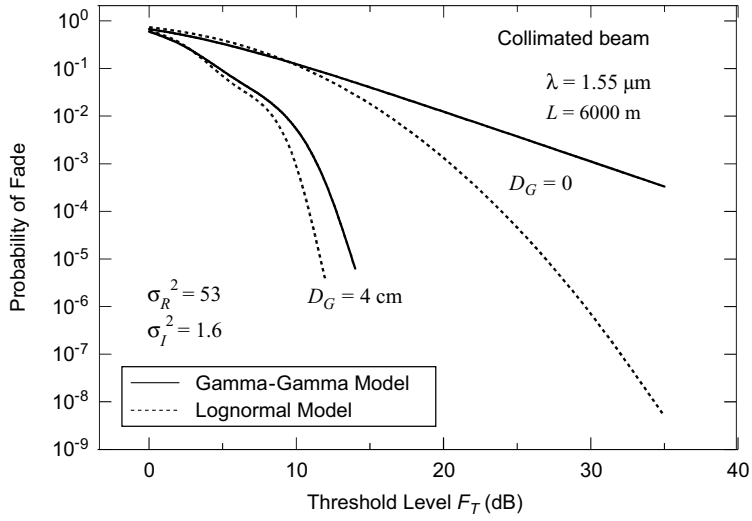

Figure 11.8 Same as Fig. 11.6 except under strong irradiance fluctuation conditions ($\sigma_R^2 \gg 1$).

The beam parameters in (29) and (30) are defined in Section 10.2, $\sigma_R^2 = 1.23 C_n^2 k^{7/6} \times L^{11/6}$ is the Rytov variance for a plane wave, and σ_B^2 is the Rytov variance for a Gaussian-beam wave [Eq. (91) in Chap. 9]. Except for a large-aperture focused beam, this last parameter can be closely approximated by the simpler expression

$$\sigma_B^2 \cong 3.86\,\sigma_R^2 \left\{ 0.40\left[(1+2\Theta_1)^2 + 4\Lambda_1^2\right]^{5/12} \times \cos\left[\frac{5}{6}\tan^{-1}\frac{1+2\Theta_1}{2\Lambda_1}\right] - \frac{11}{16}\Lambda_1^{5/6} \right\}. \tag{31}$$

In arriving at the results in Figs. 11.6–11.8, we have taken various path lengths L, but otherwise set $C_n^2 = 10^{-13}\,\mathrm{m}^{-2/3}$, $l_0 = 0$, $L_0 = \infty$, $W_0 = 1\,\mathrm{cm}$, and $\lambda = 1.55\,\mu\mathrm{m}$. The assumed path length in Fig. 11.6 is $L = 500$ m which leads to $\sigma_R^2 = 0.56$ and $\sigma_I^2 = 0.13$, respectively, in the pupil plane of the receiver. These values are characteristic of weak fluctuation conditions. In general, the lognormal model predicts lower (i.e., optimistic) fade probabilities for a given fade threshold value F_T as compared with the gamma-gamma model. In both models, the case of a large-aperture receiver shows considerable improvement in the predicted fade probability. The focusing regime is illustrated in Fig. 11.7 in which $L = 2000$ m. The resulting pupil plane Rytov variance and scintillation index are $\sigma_R^2 = 7$ and $\sigma_I^2 = 1.27$. The lognormal model in this figure is shown only for the sake of comparison. Note that a probability of fade equal to 10^{-6}, based on the gamma-gamma model and receiver aperture $D_G = 4$ cm, is achieved in Fig. 11.6 (weak fluctuations) when $F_T \cong 3.2$ dB below the mean irradiance,

whereas the same fade probability in Fig. 11.7 (focusing regime) requires $F_T \cong 23$ dB below the mean irradiance.[2] The saturation regime is characterized in Fig. 11.8 with $L = 6000$ m. Here we find the Rytov variance and scintillation index to be $\sigma_R^2 = 53$ and $\sigma_I^2 = 1.6$, respectively. Clearly, more aperture averaging (i.e., a larger aperture) is required in strong turbulence ($\sigma_R^2 \gg 1$) to compensate for the scintillation. However, in Fig. 11.8 we note that a fade probability of 10^{-6} can be achieved with $F_T \cong 15$ dB below the mean irradiance. Last, the results shown here can be readily extended to more general cases including nonzero inner scale and a finite outer scale.[3]

11.3.2 Expected number of fades

The number of negative (or positive) crossings of a prescribed threshold characterizes the *expected number of fades* per unit time $\langle n(I_T)\rangle$. The general definition of expected number of fades (or surges) given by Eq. (12) is applicable also in the present case. In the case of a lognormal distribution for the irradiance, we start with the joint PDF (13) for Gaussian statistics and make the transformation of variables

$$i = \frac{1}{2}\ln\frac{I}{\langle I\rangle}, \qquad i' = \frac{I'}{2I}, \tag{32}$$

from which we deduce the Jacobian of transformation $J = 1/(4I^2)$. Consequently, the joint PDF of irradiance and its time derivative is given by [9]

$$\begin{aligned} p_{I,I'}(I,I') &= p_I(I)p_{I'}(I'|I) \\ &= \frac{1}{\sqrt{2\pi}I\sigma_I}\exp\left\{-\frac{\left[\ln(I/\langle I\rangle) + (1/2)\sigma_I^2\right]^2}{2\sigma_I^2}\right\} \\ &\quad \times \frac{1}{2I\sqrt{2\pi b_2}}\exp\left(-\frac{I'^2}{8b_2I^2}\right), \end{aligned} \tag{33}$$

where we have made the associations $\sigma_I^2 \cong 4\sigma_i^2 = 4b_0$ and $\langle i\rangle = -\sigma_i^2$, valid under weak irradiance fluctuations. Using (33) in Eq. (12), we obtain the expected number of fades

$$\begin{aligned} \langle n(I_T)\rangle &= \frac{1}{2}\int_{-\infty}^{\infty} |I'|p_I(I_T,I')\,dI' \\ &= \nu_0 \exp\left[-\frac{((1/2)\sigma_I^2 - 0.23F_T)^2}{2\sigma_I^2}\right], \end{aligned} \tag{34}$$

[2]Of course, the mean irradiance is different in each case.

[3]The software package ALTM, available from the Ontar Corporation, 9 Village Way, North Andover, MA 01845-2000 (http://www.ontar.com.), can be used to calculate fade probabilities, mean fade time, and other beam wave statistics.

where ν_0 is the *quasi-frequency* defined by

$$\nu_0 = \frac{\sqrt{b_2}}{\pi\sigma_I} = \frac{1}{2\pi}\sqrt{-\frac{B_I''(0)}{B_I(0)}}. \quad \text{[Hz]} \tag{35}$$

For the gamma-gamma distribution, the joint PDF is also of the form given by $p_{I,I'}(I, I') = p_I(I)p_{I'}(I'|I)$, but here $p_I(I)$ is the gamma-gamma PDF. That is, the irradiance and its time derivative are not statistically independent for either the lognormal model or the gamma-gamma model. However, for the gamma-gamma model, the form of the conditional PDF for I' is unknown, but we believe it is not Gaussian. Nonetheless, it can be argued on physical grounds that it is approximately a zero-mean Gaussian PDF, and reduces to such if either $\alpha \to \infty$ or $\beta \to \infty$ [9]. Thus, in this case we write

$$\begin{aligned} p_{I,I'}(I, I') \cong{}& \frac{2(\alpha\beta)^{(\alpha+\beta)/2}}{\Gamma(\alpha)\Gamma(\beta)I}\left(\frac{I}{\langle I\rangle}\right)^{(\alpha+\beta)/2} K_{\alpha-\beta}\left(2\sqrt{\frac{\alpha\beta I}{\langle I\rangle}}\right) \\ &\times \frac{1}{2\sqrt{2\pi bI}}\exp\left(\frac{-I'^2}{8bI}\right), \qquad I > 0, \end{aligned} \tag{36}$$

from which we deduce

$$\langle n(I_T)\rangle = \frac{2\sqrt{2\pi\alpha\beta}\nu_0\sigma_I}{\Gamma(\alpha)\Gamma(\beta)}\left(\frac{\alpha\beta I_T}{\langle I\rangle}\right)^{(\alpha+\beta-1)/2} K_{\alpha-\beta}\left(2\sqrt{\frac{\alpha\beta I_T}{\langle I\rangle}}\right). \tag{37}$$

Here, $b = -\langle I\rangle B_I''(0)/4$ and the quasi-frequency is

$$\nu_0 = \frac{1}{\pi\sigma_I}\sqrt{\frac{b}{\langle I\rangle}} = \frac{1}{2\pi}\sqrt{-\frac{B_I''(0)}{B_I(0)}}. \tag{38}$$

As a final comment, we note that the quasi-frequency ν_0 roughly represents the standard deviation of the normalized irradiance temporal spectrum (treated as a PDF). Therefore, the maximum width of the spectrum can be estimated to be roughly $3\nu_0$.

11.3.3 Mean fade time

When the irradiance of the received beam wave falls below a given level I_T, the average time at which it stays below this level defines the *mean fade time* in seconds. Knowing the probability of fade and the expected number of fades per second, the mean fade time is simply a ratio of these quantities given by

$$\langle t(I_T)\rangle = \frac{\Pr(I \le I_T)}{\langle n(I_T)\rangle}. \tag{39}$$

For the lognormal model, we use Eqs. (24) and (34) to calculate the mean fade time (39), whereas for the gamma-gamma distribution the comparable expressions are given by Eqs. (26) and (37).

Although the quasi-frequency ν_0 is defined by Eq. (35) or (38), we set it to a constant value of 550 Hz in our analysis simply for the sake of making comparisons between models. The quasi-frequency affects the expected number of fades and, consequently, the mean fade time, but does not have any effect on the probability of fade.

For a terrestrial link the mean duration of fade (in seconds) is shown in Figs. 11.9–11.11 under the same conditions cited in Figs. 11.6–11.8. From these results we see that, although increasing the fade threshold level F_T by several dB can substantially reduce the probability of fade by several orders of magnitude, it does not greatly reduce the corresponding mean fade time by a corresponding amount. This is true even for the large-aperture receiver cases.

11.4 Fade Statistics—Part II

In Section 11.2 we discussed FSO systems in the presence of detector noise without atmospheric effects, and in Section 11.3 we considered optical turbulence-induced fading issues alone. By using the notion of conditional probabilities, we now consider the combined effects of optical turbulence and detector noise on FSO system performance.

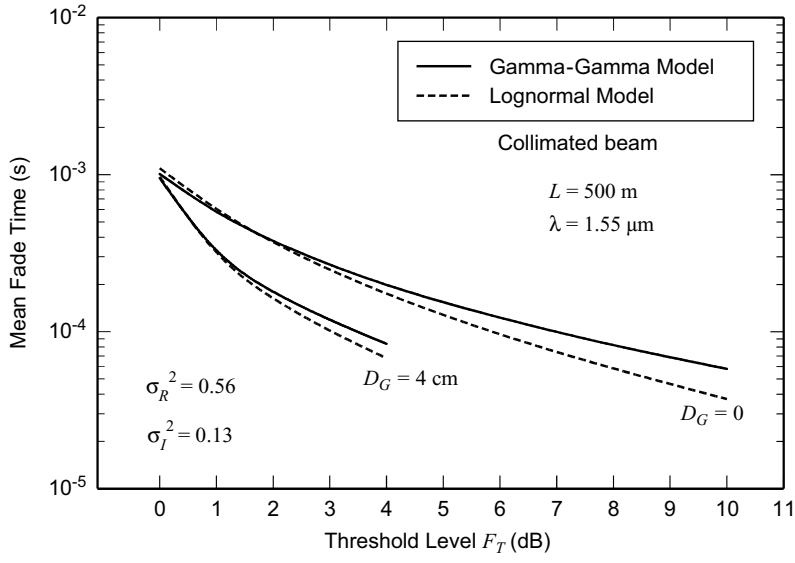

Figure 11.9 Mean duration of fade as a function of threshold level below the mean under weak irradiance fluctuation conditions ($\sigma_R^2 < 1$). Inner scale and outer scale, respectively, are assumed to be $l_0 = 0$ and $L_0 = \infty$.

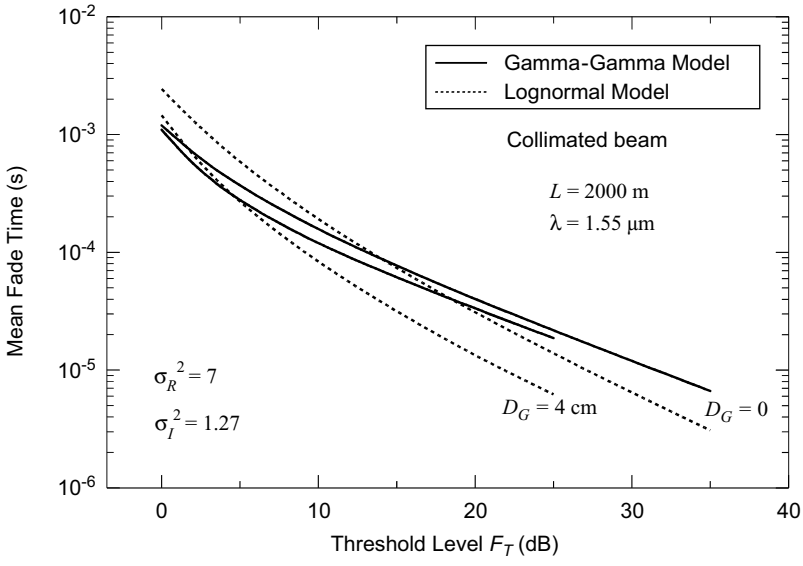

Figure 11.10 Same as Fig. 11.9 except under moderate irradiance fluctuation conditions ($\sigma_R^2 > 1$).

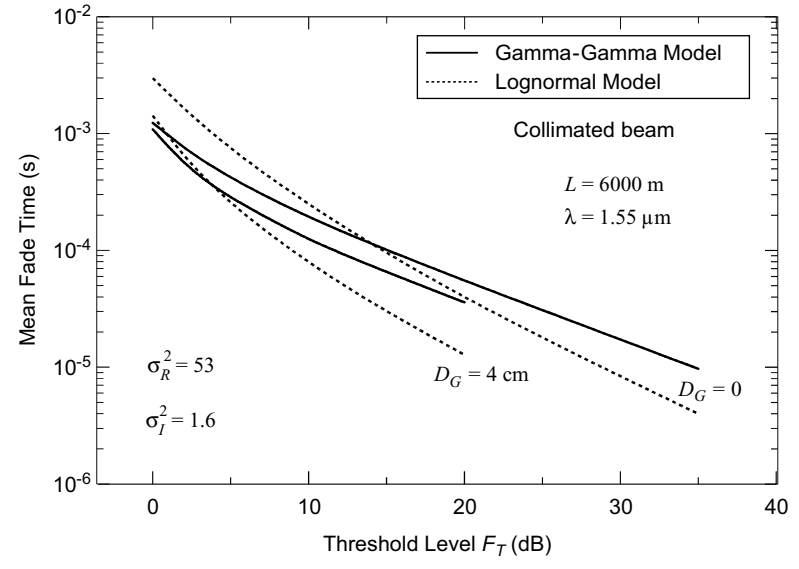

Figure 11.11 Same as Fig. 11.9 except under strong irradiance fluctuation conditions ($\sigma_R^2 \gg 1$).

11.4.1 Mean signal-to-noise ratio (SNR)

In the presence of atmospheric turbulence, the received signal exhibits additional power losses and random irradiance fluctuations. The free-space irradiance in the plane of the photodetector behind a single finite lens is given by [see Eq. (117) in Chap. 4]

$$I^0(\mathbf{r}, L + L_f) = \frac{W_0^2}{W^2(1 + \Omega_G/\Lambda_1)} \exp\left(-\frac{2r^2}{W^2}\right), \tag{40}$$

where W is the spot radius of the beam in this plane and $\Omega_G = 2L/kW_G^2$ characterizes the finite size of the lens with "soft" aperture radius W_G. If the diameter of the incident beam on the lens is much larger than the "hard" aperture diameter D_G of the lens (i.e., $\Lambda_1 \ll \Omega_G$), then we can approximate (40) quite closely by the simpler expression (see Section 4.9.2 for the relation between "soft" and "hard" apertures)

$$I^0(\mathbf{r}, L + L_f) \cong \frac{W_G^2}{W^2} I^0(0, L) \exp\left(-\frac{2r^2}{W^2}\right), \tag{41}$$

where $I^0(0, L) = W_0^2/W_1^2$ denotes the on-axis irradiance in the pupil plane.

If $I(0, L)$ denotes the instantaneous irradiance in the pupil plane of the receiver, the instantaneous input signal power on the photodetector is related by

$$P_S = \int_0^{2\pi} \int_0^{\infty} I(\mathbf{r}, L + L_f) r \, dr \, d\theta \cong \frac{1}{8} \pi D_G^2 I(0, L). \tag{42}$$

Because of random irradiance fluctuations, it follows that the output signal current i_S over long measurement intervals must be treated like a random variable. Thus, the mean signal current is represented by

$$\langle i_S \rangle = \frac{\eta e \langle P_s \rangle}{h\nu}, \tag{43}$$

where (ignoring attenuation due to absorption and/or scattering)

$$\langle P_S \rangle = \frac{1}{8} \pi D_G^2 \langle I(0, L) \rangle \cong \frac{\pi D_G^2 I^0(0, L)}{8(1 + 1.63\, \sigma_R^{12/5} \Lambda_1)}. \tag{44}$$

Following the derivation of (4), the output current from the detector $i = i_S + i_N$ in this case has mean value $\langle i_S \rangle$ and variance

$$\begin{aligned} \sigma_{SN}^2 &= \langle i_S^2 \rangle - \langle i_S \rangle^2 + \langle i_N^2 \rangle \\ &= \left(\frac{\eta e}{h\nu}\right)^2 \langle \Delta P_S^2 \rangle + \frac{2\eta e^2 B \langle P \rangle_S}{h\nu}, \end{aligned} \tag{45}$$

where $\langle \Delta P_S^2 \rangle = \langle P_S^2 \rangle - \langle P_S \rangle^2$ represents power fluctuations in the signal that become a contributor to the detector shot noise. Based on (43)–(45), the *mean*

SNR at the output of the detector in the case of a shot-noise limited system assumes the form

$$\langle \mathrm{SNR} \rangle = \frac{\langle i_S \rangle}{\sigma_{SN}} = \frac{\langle P_S \rangle}{\sqrt{\langle \Delta P_S^2 \rangle + \dfrac{2\,h\nu B \langle P_S \rangle}{\eta}}}, \tag{46}$$

which can also be rearranged as

$$\langle \mathrm{SNR} \rangle = \frac{\mathrm{SNR}_0}{\sqrt{\left(\dfrac{P_{S0}}{\langle P_S \rangle}\right) + \sigma_I^2(D_G)\mathrm{SNR}_0^2}}. \tag{47}$$

Here, SNR_0 is defined by (5), P_{S0} is the signal power in the absence of atmospheric effects, and $\sigma_I^2(D_G)$ is the irradiance flux variance on the photodetector. Thus, the power ratio $P_{S0}/\langle P_S \rangle \cong 1 + 1.63\sigma_R^{12/5}\Lambda_1$ provides a measure of SNR deterioration caused by atmospheric-induced beam spreading. Note that the reciprocal quantity $\langle P_S \rangle / P_{S0}$ is essentially the *Strehl ratio*, which is a common description of performance for an optical imaging system (see Section 14.3.5).

In Fig. 11.12 we plot the mean SNR in dB as a function of SNR_0 in dB for the special case $P_{S0}/\langle P_S \rangle = 1$ and values of $\sigma_I^2(D_G) = 0, 0.1$, and 1. Hence, in this case the mean SNR (47) reduces to

$$\langle \mathrm{SNR} \rangle = \frac{\mathrm{SNR}_0}{\sqrt{1 + \sigma_I^2(D_G)\mathrm{SNR}_0^2}}. \tag{48}$$

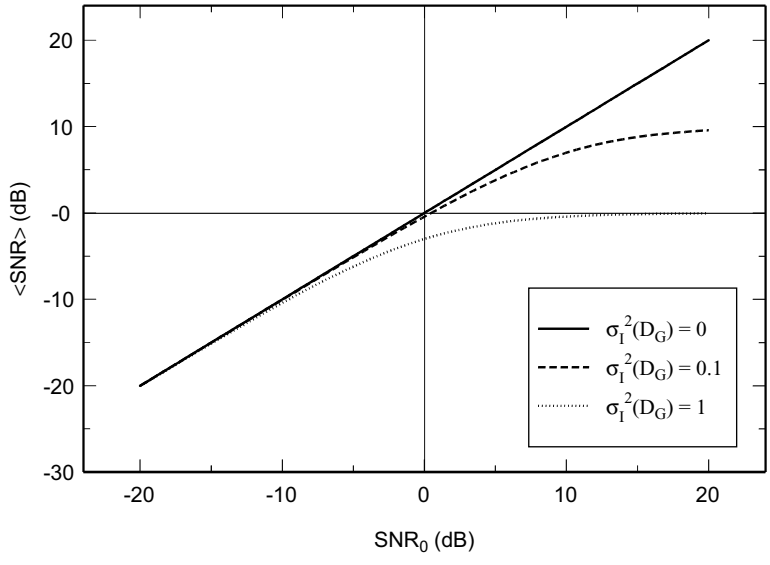

Figure 11.12 Mean signal-to-noise ratio (48) for a shot-noise limited receiver in the presence of optical turbulence. The case $\sigma_I^2(D_G) = 0$ represents no atmospheric effects.

Consequently, all degradation in mean SNR (48) is caused only by scintillation as previously pointed out by Shapiro [13]. Note that signal power fluctuations described by $\sigma_I^2(D_G)$ do not greatly affect the mean SNR system performance when SNR_0 is small (weak signal case). That is, if the signal is already weak, aperture averaging will provide little improvement in mean SNR over that for a small receiver aperture. Also, because we have assumed negligible beam spreading, the mean SNR (48) in the strong signal case will approach SNR_0 if $\sigma_I^2(D_G) \to 0$. However, for $\sigma_I^2(D_G) \neq 0$, the maximum mean SNR possible from (48) is not SNR_0 but

$$\langle \mathrm{SNR} \rangle \cong \frac{1}{\sigma_I(D_G)}, \qquad \mathrm{SNR}_0 \to \infty. \tag{49}$$

For example, to achieve $\langle \mathrm{SNR} \rangle = 20\,\mathrm{dB}$, we need $\mathrm{SNR}_0 > 20\,\mathrm{dB}$ and the irradiance flux variance must be reduced through aperture averaging to $\sigma_I^2(D_G) \leq 10^{-2}$, but to achieve $\langle \mathrm{SNR} \rangle = 30\,\mathrm{dB}$, it is necessary that aperture averaging produce $\sigma_I^2(D_G) \leq 10^{-3}$.

If we now assume the random noise in the system is a combination of background illumination, thermal noise, and electronic noise, then the noise power is defined simply by σ_N^2, the same as that which occurs in the absence of atmospheric fluctuations. In this case we define the mean SNR by

$$\langle \mathrm{SNR} \rangle = \frac{\langle i_S \rangle}{\sigma_N}. \tag{50}$$

11.4.2 False-alarm rate and fade probability

In this section we will generally treat the mean SNR as defined by Eq. (50). In the presence of turbulence-induced scintillation, we find that the required mean SNR can be much greater than that required in free space to achieve the same probability of fade (or BER). Consequently, the overall performance of a threshold detector will be adversely affected. When the fluctuation rate of incident irradiance on the receiver is small relative to the measurement sample time, we can treat the signal photocurrent i_S as essentially constant. But, because the photocurrent from sample interval to sample interval is a random variable in the presence of turbulence, the Gaussian PDF model (8) must now be taken as a conditional PDF. Hence, we can replace the signal current i_S with the random variable s and average the probability of detection (9) over the fluctuations in s, which leads to

$$\begin{aligned} \mathrm{Pr_d} &= \int_0^\infty \int_{i_T}^\infty p_I(s)\, p_{s+n}(i|s)\, di\, ds \\ &= \frac{1}{2} \int_0^\infty p_I(s) \mathrm{erfc}\left(\frac{i_T - s}{\sqrt{2}\sigma_N} \right) ds, \end{aligned} \tag{51}$$

or

$$\mathrm{Pr_d} = \frac{1}{2}\int_0^\infty p_I(u)\mathrm{erfc}\left(\frac{\mathrm{TNR} - \langle \mathrm{SNR}\rangle u}{\sqrt{2}}\right) du, \tag{52}$$

where $u = s/\langle i_S\rangle$ is the normalized signal now with unit mean and $p_I(u)$ is the PDF associated with the irradiance power fluctuations. Irrespective of the PDF model $p_I(u)$, turbulence-induced scintillation will lead to a lower detection probability calculated from (52) than that predicted by (9). Also, the related probability of fade deduced from $\mathrm{Pr_d}$ is

$$\mathrm{Pr_{fade}} = 1 - \mathrm{Pr_d} = 1 - \frac{1}{2}\int_0^\infty p_I(u)\mathrm{erfc}\left(\frac{\mathrm{TNR} - \langle \mathrm{SNR}\rangle u}{\sqrt{2}}\right) du. \tag{53}$$

Recalling Eq. (10), the probability of false alarm is

$$\mathrm{Pr_{fa}} = \frac{1}{2}\mathrm{erfc}\left(\frac{\mathrm{TNR}}{\sqrt{2}}\right), \tag{54}$$

and the related *false alarm rate* (FAR), which is the rate at which the detector noise current exceeds the receiver threshold i_T, is once again defined by [from Eq. (16)]

$$\mathrm{FAR} = \frac{B}{2\sqrt{3}}\exp\left(-\frac{\mathrm{TNR}^2}{2}\right). \tag{55}$$

To numerically evaluate the integral in (53) as a function of mean SNR, we will assume the PDF model for irradiance fluctuations is the gamma-gamma distribution (21) with unit mean written as

$$p_I(u) = \frac{2(\alpha\beta)^{(\alpha+\beta)/2}}{\Gamma(\alpha)\Gamma(\beta)} u^{(\alpha+\beta)/2-1} K_{\alpha-\beta}\left(2\sqrt{\alpha\beta u}\right), \qquad u > 0. \tag{56}$$

Specifically, we will take the case of a spherical wave for which the parameters α and β of the gamma-gamma PDF are defined explicitly by (Section 10.3.3)

$$\begin{aligned} \alpha &= \frac{1}{\exp\left[\dfrac{0.49\beta_0^2}{\left(1 + 0.18d^2 + 0.56\beta_0^{12/5}\right)^{7/6}}\right] - 1}, \\ \beta &= \frac{1}{\exp\left[\dfrac{0.51\beta_0^2(1 + 0.69\beta_0^{12/5})^{-5/6}}{\left(1 + 0.90d^2 + 0.62\,d^2\beta_0^{12/5}\right)}\right] - 1}, \end{aligned} \tag{57}$$

where $\beta_0^2 = 0.5C_n^2k^{7/6}L^{11/6}$ is the spherical wave Rytov variance. In arriving at (57), we are assuming a large receiver aperture defined by $d = \sqrt{kD_G^2/4L}$ and are neglecting the effects of both inner scale and outer scale.

In Fig. 11.13 we show the probability of fade versus the mean SNR for the case of a spherical wave with specified Rytov variance β_0^2. Here we have also specified $\mathrm{FAR}/B = 10^{-12}$, which, based on Eq. (18), yields a threshold-to-noise ratio

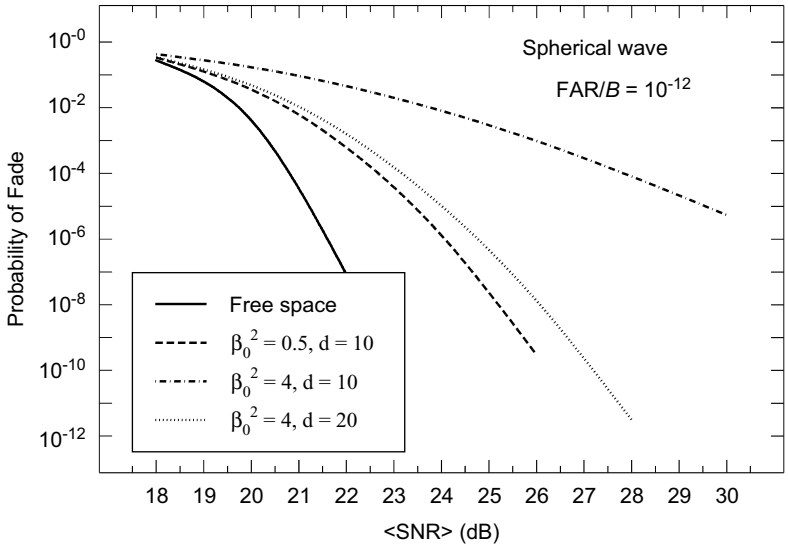

Figure 11.13 Probability of fade for a direct detection system as a function of mean SNR and various levels of scintillation and normalized aperture size $d = \sqrt{kD_G^2/4L}$. All turbulence results are based on a Kolmogorov spectrum with zero inner scale and infinite outer scale.

TNR = 7.26. The case $\beta_0^2 = 0.5$ corresponds to weak irradiance fluctuations and we have taken the receiver normalized aperture diameter $d = \sqrt{kD_G^2/4L} = 10$. For wavelength $\lambda = 1.55\,\mu$m and $C_n^2 = 5 \times 10^{-13}\,\mathrm{m}^{-2/3}$, this corresponds to a path length just over 300 m and receiver aperture $D_G \cong 3.2$ cm. For the moderate irradiance fluctuation case $\beta_0^2 = 4$, we plot the probability of fade for two normalized aperture sizes corresponding to $d = 10$ and $d = 20$. Under the conditions specified above, the path length would be roughly 1 km and aperture diameters $D_G \cong 10$ and 40 cm, respectively. For the smaller aperture case the probability of fade over the shown range of mean SNR stays significantly above any acceptable level. However, for the larger aperture size in this case we can achieve a probability of fade of roughly 10^{-6} with $\langle \mathrm{SNR} \rangle \cong 25$ dB.

11.4.3 Bit error-rate (BER) performance

In the presence of optical turbulence, the probability of error (11) is considered a conditional probability that must be averaged over the PDF of the random signal to determine the unconditional mean BER. In terms of a normalized signal with unit mean, this leads to the expression

$$Pr(E) = \langle \mathrm{BER} \rangle = \frac{1}{2}\int_0^\infty p_I(u)\mathrm{erfc}\left(\frac{\langle \mathrm{SNR} \rangle u}{2\sqrt{2}}\right)du, \tag{58}$$

where $p_I(u)$ is taken to be the gamma-gamma distribution (56) with unit mean. As in Eq. (11), we set the threshold $i_T = 0.5\,s$, so in the following analysis we are not specifying the FAR as we did in calculating fade probability.

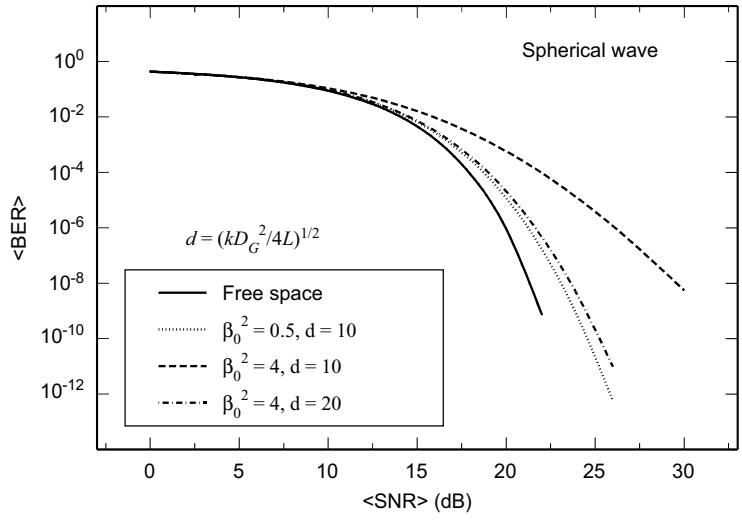

Figure 11.14 Mean probability of error (BER) for on-off keying direct detection as a function of mean SNR and various levels of turbulence. The optical wave is spherical and results are based on a Kolmogorov spectrum.

We again consider the case of a transmitted spherical wave for which the parameters of the gamma-gamma PDF are defined by (57). Numerical integration of (58) for various levels of signal fluctuation defined by $\beta_0^2 = 0.50\, C_n^2 k^{7/6} L^{11/6}$ leads to the results shown in Fig. 11.14 corresponding to the same conditions as illustrated in Fig. 11.13. Similar to the cases shown in Fig. 11.13 for the probability of fade, these results show that to achieve an acceptable level of mean BER (typically around 10^{-9}) in the presence of atmospheric turbulence, it will be necessary to utilize either a large-aperture collecting lens or, possibly, an array of small apertures (see Section 11.5).

Tyson [14] has shown that the addition of *adaptive optics* at the transmitter or receiver can also be effective in reducing the effects of scintillation and, consequently, improve system performance as measured by the BER. Under some circumstances, for example, the BER can be improved by a few orders of magnitude with the addition of adaptive optics to compensate for atmospheric-induced scintillation. Removing various Zernike modes [15] permits us to express the resulting scintillation index of a plane wave, for example, in the form

$$\sigma_I^2(L) = \frac{2.606}{2\pi} C_n^2 k^2 L \int_0^{2\pi} \int_0^{\infty} \kappa^{-8/3} \left[1 - \frac{k}{L\kappa^2} \sin\left(\frac{L\kappa^2}{k}\right)\right] \left[1 - \sum_{i=1}^{N} F_i(\kappa, D_G, \varphi)\right] d\kappa\, d\varphi, \tag{59}$$

where the filter functions in (59) are given by [16,17] (see also Section 14.5.3)

$$\left.\begin{matrix} F_i(\kappa, D_G) \\ F_{i,\text{even}}(\kappa, D_G, \varphi) \\ F_{i,\text{odd}}(\kappa, D_G, \varphi) \end{matrix}\right\} = (n+1)\left[\frac{2J_{n+1}(\kappa D_G/2)}{\kappa D_G/2}\right]^2 \left\{\begin{matrix} 1 (m=0) \\ 2\cos^2 m\varphi \\ 2\sin^2 m\varphi. \end{matrix}\right. \tag{60}$$

Although adaptive optics techniques show significant improvement in BER under weak irradiance fluctuations, aperture averaging may provide greater improvement over adaptive optics under strong irradiance fluctuations [14].

11.5 Spatial Diversity Receivers

Both direct-detection and heterodyne-detection systems associated with FSO radar and communication links can easily exhibit severe temporal short-term fading and cause phase and frequency tracking difficulties that are attributed to turbulence-induced scintillation and phase front distortions. In some situations, the loss of performance of a FSO communication system may be alleviated through increased transmitter power. However, because the power requirement in many cases may not be practical, we may instead increase the receiver aperture size for improved system performance. Nonetheless, increasing the receiver aperture size may not represent the optimum solution to the problem for a variety of practical reasons.

It has long been recognized by the radar and communications community that reliable information transmission can be realized over a fading channel with minimum transmitter power through the use of spatial diversity techniques [18–21]. That is, it is possible to achieve the spatial diversity of a large aperture by the use of several smaller apertures that are sufficiently separated so that an array of small-aperture detectors can yield the same performance as an aperture integrator receiver. Other possible direct detection diversity receivers might employ nonlinear weightings to combine the photocurrents generated by the detector array. Spatial arrays are also used in heterodyne (coherent) detection receivers. Spatial diversity through the use of multiple transmitter beams is another technique that can mitigate some of the effects of atmospheric turbulence, much like an array of receivers. The use of multiple transmitter beams is useful for uplink transmission to a satellite, for example, because conventional aperture averaging with a large aperture is not practical (see Chap. 12).

In the analysis given below we investigate the performance of a particular array of direct detection receivers as illustrated in Fig. 11.15. Such a technique is called a postdetection linear combining method, and although launching the received signal into optical fibers before detection may offer some engineering advantages, this is not necessary in the following analysis.

11.5.1 Aperture averaging using array receivers

Let the summed output of M statistically independent detectors be described by

$$i = \sum_{j=1}^{M} (i_{S,j} + i_{N,j}), \tag{61}$$

where each i_S is a random signal and each i_N is a zero-mean noise current. For simplicity we assume the mean and variance of each signal and noise current is

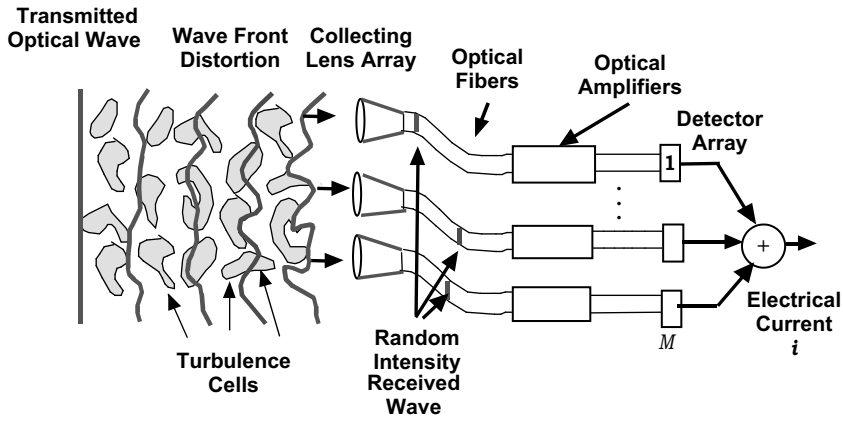

Figure 11.15 Array of M direct detection receivers.

identical. It follows therefore that the mean and variance of the total current are given by

$$\langle i\rangle = M\langle i_{S,1}\rangle, \quad \sigma_i^2 = M\Big[\langle i_{S,1}^2\rangle - \langle i_{S,1}\rangle^2 + \langle i_{N,1}^2\rangle\Big] = M\big(\sigma_{S,1}^2 + \sigma_{N,1}^2\big), \tag{62}$$

and hence, we conclude that the mean rms amplitude SNR is simply

$$\langle \mathrm{SNR_M}\rangle = \frac{M\langle i_{S,1}\rangle}{\sqrt{M(\sigma_{S,1}^2 + \sigma_{N,1}^2)}} = \sqrt{M}\langle \mathrm{SNR}_1\rangle, \tag{63}$$

where $\langle \mathrm{SNR}_1\rangle$ is the mean SNR of a single detector.

The above analysis shows that the output SNR from an array of M detectors can improve the output SNR of a single detector by the factor $\sqrt{M}$. Likewise, the scintillation index of the summed output is reduced by M, i.e.,

$$\sigma_{I,M}^2 = \frac{1}{M}\sigma_{I,1}^2. \tag{64}$$

However, to compare the performance of an array of small-aperture detectors in reducing scintillation with that of a single large-aperture detector, we consider the case where the receiver collecting aperture area of the M small receiver apertures is equal to the area of a single large aperture. Hence, if D_G is the diameter of the large aperture and D_1 is the diameter of each small aperture, then $D_G^2 = MD_1^2$.

For the sake of comparing the aperture averaging effect of an array with that of a single monolithic aperture as provided in Section 10.3, we ignore noise in the detector and compare aperture-averaging factors for the case of an infinite plane wave propagating through atmospheric turbulence along a horizontal path with

negligible inner scale and infinite outer scale. For the large-aperture detector, the aperture-averaging factor is defined by

$$A = \frac{\sigma_I^2(D_G)}{\sigma_I^2(0)}, \tag{65}$$

where the flux variance for a plane wave is given by Eq. (69) in Chap. 10. This same equation is also valid for each of the small apertures of the array with D_G replaced by $D_G/\sqrt{M}$ and the aperture averaging factor of the summed output is obtained from (65) divided by the number of apertures M, i.e.,

$$A_M = \frac{\sigma_I^2\left(D_G/\sqrt{M}\right)}{M\sigma_I^2(0)}. \tag{66}$$

The resulting aperture averaging factors for the single aperture system and the array system are shown in Figs. 11.16–11.18 for M=1, 2, 5, and 10 apertures and several values of the Rytov variance corresponding to weak fluctuations, moderate fluctuations, and strong fluctuations of the irradiance. All results are based on a Kolmogorov spectrum with $l_0 = 0$ and $L_0 = \infty$. The case $M = 1$ corresponds to a single large aperture. If the size of the individual apertures exceeds the irradiance correlation width, some aperture averaging will occur in each small aperture, but they will otherwise act as point detectors. Also, as a consequence of Eq. (66), the array always has a smaller aperture averaging coefficient than the single large-aperture case until the single-aperture radius is roughly 10 times the size of the

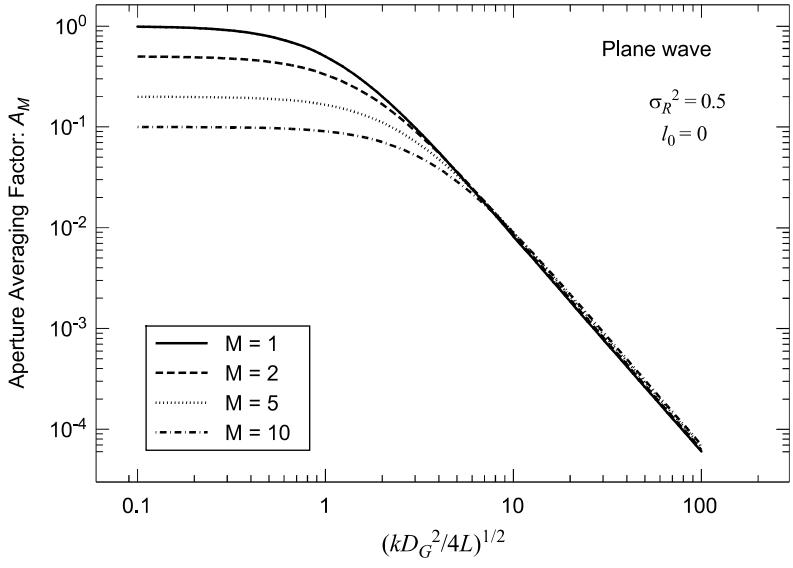

Figure 11.16 Comparison of the predicted aperture-averaging factor for a single aperture ($M = 1$) and an array of small apertures for the case of a plane wave in weak irradiance fluctuations. In all cases the glass area of the M collecting lenses is the same as that of the single large lens.

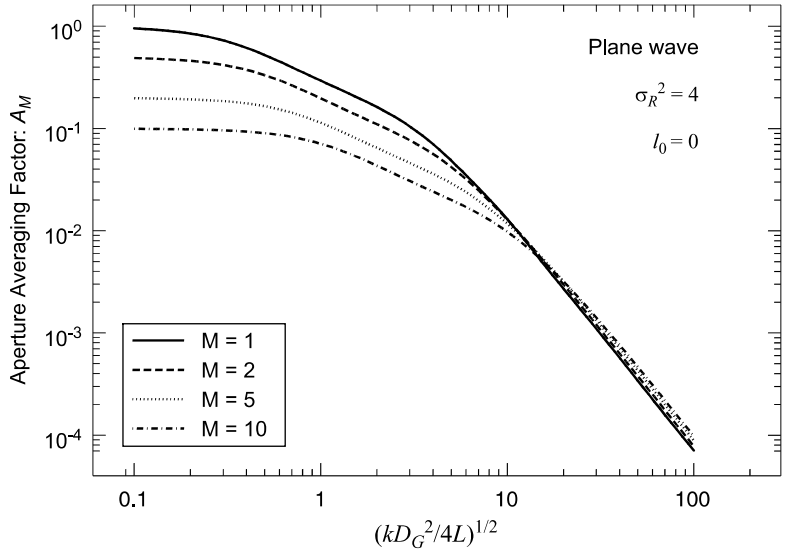

Figure 11.17 Same as Fig. 11.16 for moderate fluctuations.

Fresnel zone or more. After that the aperture averaging coefficient of the single large aperture decreases more rapidly than the total area of the M collecting lenses increases, and thus predicts a somewhat smaller aperture-averaging coefficient than that of the array. This is a consequence of the fact that aperture-averaging effects with a single large aperture decrease with $1/D_G^{7/3}$ [for example, recall Eq. (61) in Chap. 10], whereas the array for our case decreases with $1/D_G^2$.

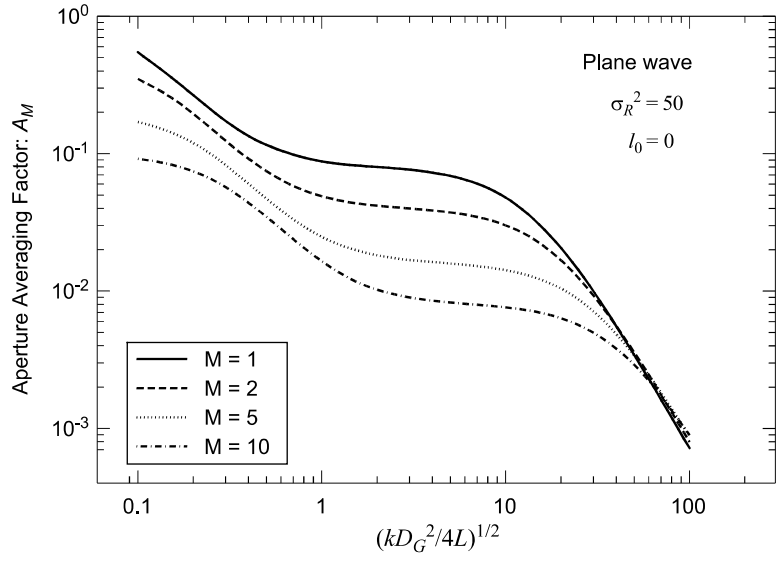

Figure 11.18 Same as Fig. 11.16 for strong fluctuations.

11.5.2 Bit error-rate (BER) performance

Evaluation of the BER performance associated with an array of direct detection receivers as given below is based on the following simplifying assumptions:

- the aperture diameter of each receiver in the array is less than the spatial correlation width of the irradiance fluctuations so that each receiver acts like a "point detector."
- the array elements are spatially separated by a sufficient distance that each acts independently of the others.
- the summed output of the array can be reasonably approximated by a gamma-gamma distribution.

In addition, we will compare the mean BER corresponding to $M = 1$, 5, and 10 apertures given that the mean SNR is the same in each case.

For M apertures in the array system, the scintillation index is related to the parameters α_M and β_M of the gamma-gamma PDF by

$$\sigma_{I,M}^2 = \left(1 + \frac{1}{\alpha_M}\right)\left(1 + \frac{1}{\beta_M}\right) - 1, \quad M = 1, 2, 3, \ldots. \tag{67}$$

Because of Eq. (64) and the fact that scintillation is caused primarily by small-scale inhomogeneities, we argue now that the small-scale scintillation index associated with the summed output of the array is roughly the small-scale scintillation index of a single aperture output divided by the number of apertures M. In this case we define the parameters α_M and β_M for the summed output by

$$\alpha_M = \frac{1 + M\beta_1}{M\beta_1\sigma_{I,M}^2 - 1}, \quad \beta_M = M\beta_1, \ \ M = 1, 2, 3, \ldots. \tag{68}$$

As in Section 11.4.3, we will assume that Eq. (58) describes the probability of error for an OOK system. In Figs. 11.19 and 11.20, respectively, we show the implied mean BER as a function of $\langle \mathrm{SNR_M} \rangle$ for weak fluctuation conditions ($\beta_0^2 = 0.5$) and moderate fluctuation conditions ($\beta_0^2 = 4$), given that the transmitted optical wave is a spherical wave. Once again, we have ignored the effects of inner scale and outer scale. It is difficult to make direct comparison of the results in Figs. 11.19 and 11.20 for an array system with the single large-aperture receiver system shown in Fig. 11.14 because we cannot equate $\langle \mathrm{SNR_M} \rangle$ for the array system with $\langle \mathrm{SNR} \rangle$ for the single-aperture system. Nonetheless, we see that the mean BER for the array system can be reduced by several orders of magnitude by increasing the number of apertures from one to ten, given a fixed value of mean $\mathrm{SNR_M}$. A similar observation was made concerning an array of coherent receivers in which such improvement was established by experimental data and the same PDF model [9].

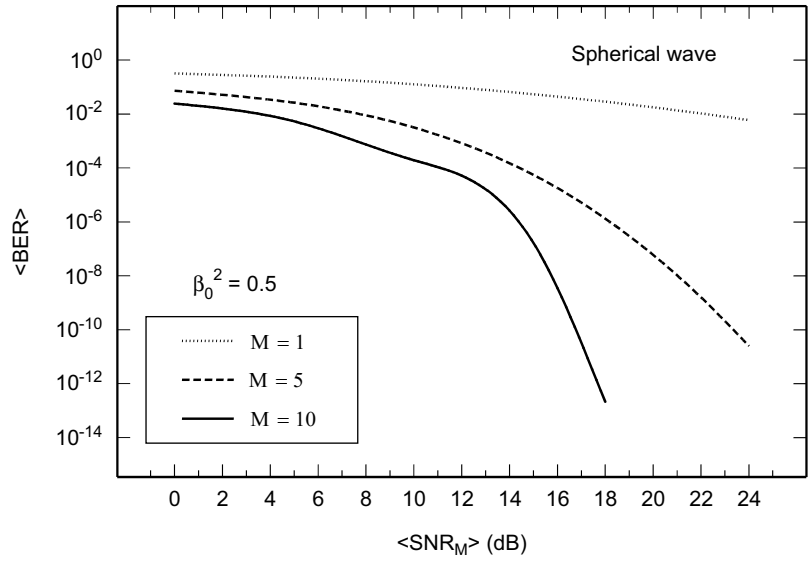

Figure 11.19 The BER for an array of *M* direct detection receivers as a function of mean SNR under weak fluctuation conditions.

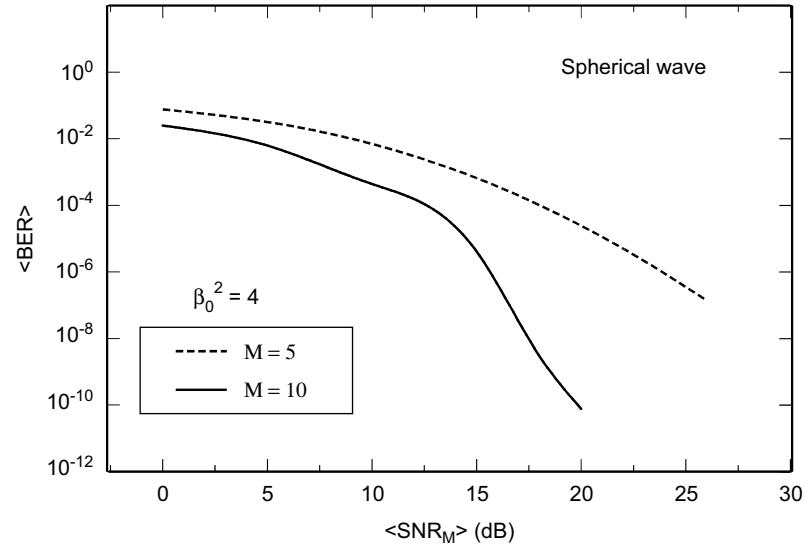

Figure 11.20 The BER for an array of *M* direct detection receivers as a function of mean SNR under moderate fluctuation conditions.

11.6 Summary and Discussion

Here we summarize only the key tools and ideas of this chapter. Because traditional copper wires and coaxial cables that are commonly used to connect buildings to telephone and cable television cannot offer the gigabit-per-second capacity required by certain high-performance systems, there is now renewed emphasis on FSO systems that utilize low-power infrared laser transceivers that can beam two-way data at gigabit-per-second rates. However, *optical turbulence* is generally considered the limiting factor in the performance of such a FSO communication link.

Performance measures of FSO communication systems depend strongly on the SNR that, for a shot-noise limited system in the absence of optical turbulence, takes the form

$$\mathrm{SNR}_0 = \sqrt{\frac{\eta P_S}{2h\nu B}}, \tag{69}$$

where P_S is the signal power and B is the bandwidth. For a given signal i_S and specified threshold i_T, the *probability of detection* and *probability of false alarm* are defined, respectively, by

$$\mathrm{Pr_d} = \int_{i_T}^{\infty} p_{s+n}(i)\, di = \frac{1}{2}\mathrm{erfc}\left(\frac{i_T - i_S}{\sqrt{2}\sigma_N}\right), \tag{70}$$

$$\mathrm{Pr_{fa}} = \int_{i_T}^{\infty} p_n(i)\, di = \frac{1}{2}\mathrm{erfc}\left(\frac{i_T}{\sqrt{2}\sigma_N}\right). \tag{71}$$

In arriving at these results we have used a Gaussian model for noise where σ_N^2 is the noise power.

In the presence of atmospheric turbulence, it is customary to describe system performance not in terms of probability of detection, but in terms of the related *probability of fade*. If the free-space SNR is sufficiently high, then the fade probability is determined by atmospheric effects alone. In this case it is defined by

$$\mathrm{Pr_{fade}} = P(I \le I_T) = \int_0^{I_T} p_I(I)\, dI, \tag{72}$$

where $p_I(I)$ is the PDF of the fluctuating irradiance and I_T is the threshold. When noise in the system is considered as well as atmospheric effects, we use conditional statistics to calculate various fade parameters. In particular, the probability of fade is now defined by

$$\mathrm{Pr_{fade}} = 1 - \frac{1}{2}\int_0^{\infty} (u)\mathrm{erfc}\left(\frac{\mathrm{TNR} - \langle \mathrm{SNR}\rangle u}{\sqrt{2}}\right) du, \tag{73}$$

where TNR denotes the *threshold-to-noise ratio* (17) and $\langle \text{SNR} \rangle$ is the *mean signal-to-noise ratio.* Similarly, the *bit error rate* (BER) under the same conditions leads to

$$\Pr(E) = \langle \text{BER} \rangle = \frac{1}{2} \int_0^\infty p_I(u) \text{erfc}\left(\frac{\langle \text{SNR} \rangle u}{2\sqrt{2}} \right) du, \tag{74}$$

where we have assumed a simple *on-off keying* (OOF) modulation technique.

11.7 Worked Examples

Example 1: Consider a FSO communication system operating over a 2 km link along a horizontal path. Assume the transmitter uses a 4 cm diameter collimated beam operating at wavelength $\lambda = 1.55$ μm and the receiver aperture diameter is 10 cm. Also, assume $C_n^2 = 7 \times 10^{-14}\,\text{m}^{-2/3}$ and use a Kolmogorov spectrum to calculate the following:

(*a*) the scintillation index in the plane of the receiver.
(*b*) the scintillation index in the plane of the detector.
(*c*) What is the fade probability (gamma-gamma PDF) for a threshold below mean of $F_T = 6$ dB?
(*d*) Keeping all parameters the same except the link is now 4 km, what is the corresponding probability of fade?
(*e*) For part (*d*), what fade threshold F_T will ensure a fade probability of 10^{-6}?
(*f*) If the link is 4 km and $F_T = 6$ dB, what size receiver aperture is necessary to ensure a fade probability of 10^{-6}?

Solution: We first calculate the quantities (for 2 km path):

$$\Theta_0 = 1 - \frac{L}{F_0} = 1, \quad \Lambda_0 = \frac{2L}{kW_0^2} = 2.4669, \quad \sigma_R^2 = 1.23 C_n^2 k^{7/6} L^{11/6} = 4.97$$

$$\Theta_1 = \frac{\Theta_0}{\Theta_0^2 + \Lambda_0^2} = 0.1411, \quad \Lambda_1 = \frac{\Lambda_0}{\Theta_0^2 + \Lambda_0^2} = 0.3482,$$

$$\Omega_G = \frac{2L}{kW_G^2} = \frac{16L}{kD_G^2} = 0.7894$$

$$\sigma_B^2 \cong 3.86\ \sigma_R^2 \left\{ 0.40 \left[(1 + 2\Theta_1)^2 + 4\Lambda_1^2 \right]^{5/12} \cos\left[\frac{5}{6} \tan^{-1}\left(\frac{1 + 2\Theta_1}{2\Lambda_1} \right) \right] - \frac{11}{16} \Lambda_1^{5/6} \right\} = 1.106.$$

(*a*) $\sigma_I^2(0) = \exp[\sigma_{\ln x}^2(0) + \sigma_{\ln y}^2(0)] - 1 = 0.93$
(*b*) $\sigma_I^2(D_G) = \exp[\sigma_{\ln x}^2(D_G) + \sigma_{\ln y}^2(D_G)] - 1 = 0.051$

(*c*) The parameters of the gamma-gamma PDF are $\alpha = 45.94, \beta = 35.01$, and thus

$$\Pr_{\text{fade}} = P(I \leq I_T) = \int_0^{I_T} p_I(I)\, dI = 3.28 \times 10^{-8}.$$

(*d*) $\Pr_{\text{fade}} = P(I \leq I_T) = 1.09 \times 10^{-2}$.
(*e*) $F_T = 14.7$ dB below the mean irradiance.
(*f*) $D_G = 17.2$ cm.

❑

Problems

Section 11.2

1. For a detection system in which $\Pr_{fa} = 10^{-6}$, what is the required SNR_0 to ensure a detection probability of $\Pr_d = 0.999$?
   Ans. $SNR_0 = 18$ dB
2. For the required SNR_0 in Prob. 1, what is the corresponding BER?
3. If we specify $FAR/B = 10^{-11}$ for a direct detection system,
   (*a*) What is the corresponding TNR?
   (*b*) What is the required SNR_0 to ensure a detection probability of $\Pr_d = 0.999$?
4. Repeat Prob. 3 for the case in which $FAR/B = 10^{-9}$.

Section 11.3

5. Solve Example 1 in Section 11.7 using the lognormal PDF for irradiance.
6. Given a propagation distance of 3 km but otherwise assume the conditions stated in Example 1 in Section 11.7, use the lognormal PDF model to calculate
   (*a*) the probability of fade.
   (*b*) the expected number of fades if $\nu_0 = 100$ Hz.
   (*c*) the mean fade time.

Section 11.4

7. Assume a spherical wave with $\lambda = 1.55\,\mu$m is propagated over a horizontal path to a direct detection receiver 1 km from the source. If $C_n^2 = 5 \times 10^{-14}\,\mathrm{m}^{-2/3}$, use a Kolmogorov spectrum and the lognormal PDF to calculate the probability of fade when
   (*a*) $D_G = 15$ cm, TNR = 7, and $\langle \mathrm{SNR} \rangle = 25$ dB.
   (*b*) Repeat part (*a*) when $C_n^2 = 5 \times 10^{-13}\,\mathrm{m}^{-2/3}$.
8. Repeat Prob. 7 using the gamma-gamma PDF for irradiance.
9. Assume a spherical wave $\lambda = 1.55\,\mu$m is propagated over a horizontal path to a direct detection receiver 1 km from the source. If $C_n^2 = 5 \times 10^{-14}\,\mathrm{m}^{-2/3}$, use a Kolmogorov spectrum and the lognormal PDF to calculate the BER given that
   (*a*) $D_G = 15$ cm and $\langle \mathrm{SNR} \rangle = 25$ dB.
   (*b*) $D_G = 15$ cm and $\langle \mathrm{SNR} \rangle = 30$ dB.
10. Repeat Prob. 9 for a Gaussian-beam wave in which the diameter of the exit aperture of the transmitter is 2 cm.

References

1. W. B. Davenport and W. L. Root, *An Introduction to the Theory of Random Signals and Noise*, McGraw-Hill, New York (1958).
2. R. M. Gagliardi and S. Karp, *Optical Communications*, 2nd ed. (John Wiley & Sons, New York, 1995).
3. R. H. Kingston, *Optical Sources, Detectors, and Systems: Fundamentals and Applications*, Academic Press, San Diego (1995).
4. S. B. Alexander, *Optical Communication Receiver Design* (SPIE Optical Engineering Press, Bellingham, Wash., 1997).
5. S. O. Rice, "The mathematical analysis of random noise," *Bell Sys. Tech. J.* **23**, 282–332 (1944); **24**, 46–156 (1945).
6. S. O. Rice, "Statistical properties of a sine wave plus random noise," *Bell Sys. Tech. J.* **27**, 109–158 (1948).
7. P. Beckmann, *Probability in Communication Engineering* (Harcourt, Brace & World, New York, 1967).
8. R. J. Hill, R. G. Frehlich, and W. D. Otto, "The probability distribution of irradiance scintillation," NOAA Tech. Memo. ERL ETL-274 (NOAA Environmental Research Laboratories, Boulder, CO, 1996).
9. L. C. Andrews, R. L. Phillips, and C. Y. Hopen, *Laser Beam Scintillation with Applications* (SPIE Optical Engineering Press, Bellingham, Wash., 2001).
10. R. J. Hill and R. G. Frehlich, "Probability distribution of irradiance for the onset of strong scintillation," *J. Opt. Soc. Am. A* **14**, 1530–1540 (1997).
11. S. M. Flatté, C. Bracher, and G.-Y. Wang, "Probability-density functions of irradiance for waves in atmospheric turbulence calculated by numerical simulations," *J. Opt. Soc. Am. A* **11**, 2080–2092 (1994).
12. M. A. Al-Habash, L. C. Andrews, and R. L. Phillips, "Mathematical model for the irradiance PDF of a laser beam propagating through turbulent media," *Opt. Eng.* **40**, 1554–1562 (2001).
13. J. H. Shapiro, "Imaging and optical communication through atmospheric turbulence," in *Laser Beam Propagation in the Atmosphere*, J. W. Strohbehn, ed. (Springer, New York, 1978).
14. R. K. Tyson, "Bit-error rate for free-space adaptive optics laser communications," *J. Opt. Soc. Am. A* **19**, 753–758 (2002).
15. R. K. Tyson, *Principles of Adaptive Optics* (Academic Press, San Diego, 1991).
16. R. J. Sasiela, *Electromagnetic Wave Propagation in Turbulence* (Springer, New York, 1994).
17. L. C. Andrews and R. L. Phillips, *Mathematical Techniques for Engineers and Scientists* (SPIE Optical Engineering Press, Bellingham, Wash., 2003).
18. M. Schwartz, W. R. Bennet, and S. Stein *Communication Systems and Techniques* (IEEE Press New York, 1996); [formerly published by McGraw-Hill, (1966)].

19. S. Resenberg and M. C. Teich, "Photocounting array receivers for optical communication through the lognormal atmospheric channel. 2: Optimum and suboptimum receiver performance for binary signaling," *Appl. Opt.* **12**, 2625–2635 (1973).
20. J. H. Churnside and M. C. McIntyre, "Averaged threshold receiver for direct detection of optical communications through the lognormal atmospheric channel," *Appl. Opt.* **16**, 2669–2676 (1977).
21. A. Belmonte, A. Comerón, J. A. Rubio, J. Bará, and E. Fernández, "Atmospheric-turbulence-induced power-fade statistics for a multiaperture optical receiver," *Appl. Opt.* **36**, 8632–8638 (1997).